Predictive Value of Fundus Autofluorescence for Development of Geographic Atrophy in Age-Related Macular Degeneration

John Chopin Hwang, Jackie W. K. Chan, Stanley Chang, and R. Theodore Smith

Purpose. It has been suggested that lipofuscin accumulation, as measured by increased fundus autofluorescence (FAF), precedes progression or development of junctional zone geographic atrophy (GA) in age-related macular degeneration (AMD). The tools of biomedical image analysis were used to measure the probabilistic relationship of GA progression to increased FAF.

Methods. Serial AF images of eight eyes of six patients with AMD with GA were registered on computer. The images were leveled with a 12-zone quadratic polynomial mathematical model to minimize background variability. Semiautomated segmentation of GA was performed on the leveled images. Increased FAF was defined as a gray level greater than 2 standard deviations above the leveled image mean, identified on the initial image with automated segmentation, and measured as a fraction of the 250-μm border zone surrounding the initial GA lesion. Areas of GA lesions were identified on the final image. The positive predictive value (PPV) of increased FAF was determined as the probability that any pixel with increased FAF in the initial image would become part of new GA in the final image. Relative PPV was determined relative to the total quantity of new GA. The NPV (NPV) of increased FAF was calculated as the probability that any pixels without increased FAF would not become atrophic. The relative NPV was determined similarly. A similar analysis was also conducted with a 500-μm border zone to determine the predictive value of proximity to the original GA lesion ("proximity") for GA progression.

Results. As a fraction of the geographic atrophy border zone, the mean new GA was 0.44 $\pm$ 0.20, and the mean increased FAF was 0.06 $\pm$ 0.06. The mean PPV of increased FAF for new GA formation was 0.50 $\pm$ 0.26. Compared with the relative PPV of chance of 1.0, the mean relative PPV of increased FAF was 1.15 $\pm$ 0.28. The mean NPV of increased FAF was 0.57 $\pm$ 0.20. The mean relative NPV of increased FAF was 1.00 $\pm$ 0.02. In the 500-μm border zone, the mean relative PPV of FAF and of proximity were essentially equal (1.56 $\pm$ 0.70 and 1.52 $\pm$ 0.26, respectively), whereas the mean relative NPV of proximity was significantly greater than that of FAF (1.26 $\pm$ 0.19 and 1.01 $\pm$ 0.01, respectively, $P = 0.02$)

Conclusions. The results of digital image analysis suggest that although increased FAF may have a modest PPV for new GA development, the relative PPV is generally no greater than chance. Similarly, the relative NPV demonstrates negligible difference from chance and is also lower than the relative NPV of proximity. This suggests that increased FAF, though a disease manifestation, is not a strong risk factor for development or extension of GA. (*Invest Ophthalmol Vis Sci.* 2006;47: 2655–2661) DOI:10.1167/iovs.05-1027

There is considerable interest in the effect of lipofuscin on retinal pigment epithelium (RPE) function and its role in retinal diseases. Lipofuscin granules accumulate with age in postmitotic RPE lysosomal compartments as phagocytic remnants of photoreceptor outer segment discs.[1–5] Previous studies suggest that lipofuscin and its constituent A2E may exert toxic effects on normal RPE cellular processes.[5–10] Lipofuscin granules also accumulate more rapidly in monogenic retinal disorders, such as Best disease and Stargardt disease, and complex degenerative diseases such as age-related macular degeneration (AMD).[11–14] However, the precise influence of these granules remains uncertain.

Lipofuscin accumulation has been examined in vivo with fundus autofluorescence (FAF), by confocal scanning laser ophthalmoscopy. Several studies demonstrate that hyperfluorescent FAF signals are reliable markers of lipofuscin in RPE cells.[15–18]

Abnormal lipofuscin accumulation occurs in age-related macular degeneration (AMD), the most common cause of legal blindness in developed countries.[19] Visual loss is generally attributed to choroidal neovascularization and RPE detachment. However, geographic atrophy (GA) of RPE accounts for 12% to 21% of severe visual loss.[20–23] Junctional zones of GA can demonstrate abnormal FAF patterns, indicating localized accumulation of lipofuscin.[18] The importance of this phenomenon remains unclear. However, a previous study based on a small case series of three patients suggests that areas of increased FAF may precede development or enlargement of GA.[24]

The goal of this study is to determine whether lipofuscin accumulation, as measured by increased FAF, is a precursor of GA progression. This determination will be made by digitally analyzing serial FAF images in patients with GA and quantifying changes in junctional zone atrophy.

Methods

Patient Selection and Image Acquisition

AF images of eight eyes of six patients with GA were selected retrospectively from a database of patients imaged from 2002 to 2005 at Columbia University. All eyes had drusen as well as GA. Each eye had an initial and a final AF image representing a follow-up of 2 to 3 years. The ages of the patients ranged from 76 to 82 years with a median of 78. The dataset included three males and three females, all white.

After pupillary dilation, fundus AF images had been recorded using the Heidelberg model HRA confocal scanning laser ophthalmoscope (SLO; Heidelberg Inc, Heidelberg, Germany). This instrument uses blue laser light at 488 nm for illumination and a barrier filter at 500 nm, to limit the captured light to autofluorescent structures. The AF images

From the Department of Ophthalmology, Columbia University, New York, New York.

Supported by a grant from The New York Community Trust (RTS) and unrestricted funds from Research to Prevent Blindness.

Submitted for publication August 3, 2005; revised September 27 and October 25, 2005; accepted January 12, 2006.

Disclosure: **J.C. Hwang**, None; **J.W.K. Chan**, None; **S. Chang**, None; **R.T. Smith**, None

The publication costs of this article were defrayed in part by page charge payment. This article must therefore be marked "*advertisement*" in accordance with 18 U.S.C. §1734 solely to indicate this fact.

Corresponding author: R. Theodore Smith, Department of Ophthalmology, Columbia University, 635 West 165 St., #314, New York, NY 10032; rts1@columbia.edu.

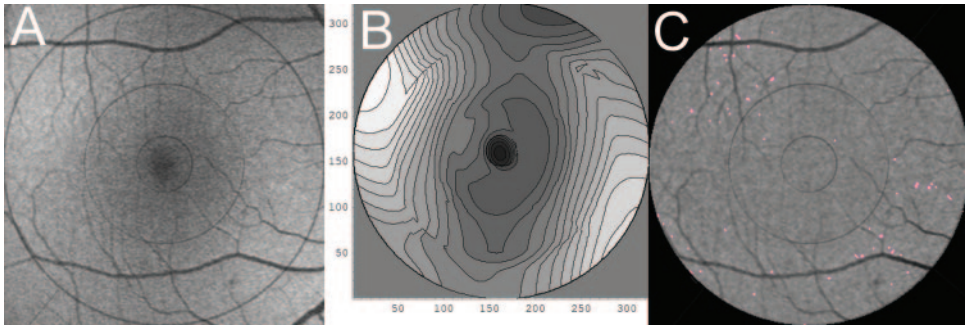

FIGURE 1. Mathematical model and segmentation of a normal AF scan. (**A**) Right eye of 54-year-old woman showing significant background variability and foveal decreased fluorescence due largely to luteal pigment. (**B**) Twelve-zone mathematical model of the AF background in (**A**), presented as a contour graph. Note how the model captures the background variability of the original scan. It is essentially smooth throughout with the exception of a residual mild discontinuity superotemporally in this blend zone. The contour lines are closer together in the fovea where the background is more highly variable. (**C**) The image in (**A**) leveled by subtracting the model in (**B**). The background of the leveled image is now homogeneous, with a mean gray level of 126 ± 11.6 (SD). The global threshold of 2.0 standard deviations above the mean defining increased FAF was therefore 149.2, which was applied to the entire leveled image and yielded the increased FAF shown in pink (0.28% of the 6000-μm zone). Comparison of the increased FAF with the original image (**A**) demonstrates a very reasonable selection. By contrast, the use of any single threshold in the unleveled image (**A**) to define increased FAF would cause major errors, due to the image variability.

consisted of bitmapped laser scans, 512 × 512 pixels in size, centered on the macula. Each image was an average of three to six scans composed by the SLO software. We required good quality in the initial images so that increased FAF would be well characterized. We allowed fair quality in the final image if the GA could be well defined and there were sufficient details for image registration. All images had a scale of approximately 15 μm per pixel. For processing and analysis, the images were imported into image-analysis software (Photoshop 7.0; Adobe Systems, Inc., Mountain View, CA) as bitmapped files consisting of 256 gray levels for each pixel. The image was then cropped to a 6000-μm square centered on the fovea. All subsequent analyses were performed on these images.

The study adhered to the tenets of the Declaration of Helsinki and received approval by the institutional review board of New York Presbyterian Hospital (New York, NY).

Image Analysis

Images were classified by FAF phenotype patterns in accordance with recently published guidelines.[25]

To make quantitative assessments of abnormal AF relative to the image background, and to perform this thresholding efficiently and uniformly in the setting of significant background variability, the AF image was leveled with a 12-zone quadratic polynomial mathematical model of the background in a manner analogous to that previously described for drusen segmentation.[26] The model was tested for accuracy on normal AF scans, as will be described. The details of implementation for GA and increased FAF then follow.

For the fovea, we had previously found that the geometry of normal AF images was affected by the absorption of 488-nm blue light by luteal pigment, in much the same manner that the green channel of a fundus photograph is affected. Thus, in the fovea, properly filtered normal AF images exhibited concentric elliptical isobars of fluorescence, with fluorescence increasing outward along any radius from a least-fluorescent center. Furthermore, a two-zone quadratic polynomial model could fit foveal AF data with mean absolute errors ranging from 3.6% ± 3.7% to 7.3% ± 7.1% of net image range.[27] An extension of this model to the entire macula was then performed with similar accuracy (Chan JK et al. *IOVS* 2005;46:ARVO E-Abstract 4300). We describe herein the extended model version used for this study.

The 12-Zone Automated Model for Autofluorescence Images in the 6000-μm Region

We used a 600-μm central disc, three annular zones (600–1000, 1000–2000, and 2000–3000 μm diameter), and two outer annular zones (3000–4500 and 4500–6000 μm). The two outer zones were subdivided into four quadrants, giving 8 outer zones, and thus 12 zones in all. The two-threshold method of Otsu[28] was used throughout to define candidate regions in each zone with increased and decreased fluorescence, and local quadratic polynomials were fit to the remaining pixel values, as described in a previously published study.[26] Specifically, the two-threshold Otsu method was applied in each zone to provide an initial segmentation by thresholds k and m into three desired classes: C_0 (nonbackground sources with decreased autofluorescence, e.g., vessels), C_1 (background), and C_2 (areas of increased fluorescence). Because increased FAF was generally in low density, the class C_2 was further subdivided by the one-threshold Otsu method into two classes. The higher pixel values became the new C_2, and the remainder was included in C_1. This method was analogous to the analysis of a low-density drusen image.[26] For each zone, we then had an initial choice of background (C_1) for input to the quadratic polynomial background model. The resultant global model was formed from the 12 local models with appropriate radial and angular cubic spline interpolations at interfaces.

This model of macular background was fit to 10 normal AF images from 10 subjects with normal dilated retinal examinations. The average absolute errors were 3.8% ± 3.5% of net image range. The mean local standard deviations of the original images in each zone (exclusive of the hypofluorescent and hyperfluorescent pixels) ranged from 3.0% to 4.1% over the 10 images. If these mean local standard deviations are taken as representative of noise in the image, it follows that the errors of the model were of the same magnitude as the noise in the original data. Each AF image was then leveled by subtracting its background model with an offset of 125 gray levels, and the mean and SD σ of the leveled image (excluding vessels) was calculated. We found that the leveled image fell within 2.0 σ of the mean for 99.7% of pixels in each of the images (Fig. 1). (By contrast, if the gray levels of the image had a normal distribution, then gray levels above 2.0 σ would comprise 2.3% of the image.) We therefore defined increased FAF in this study as a gray level greater than 2.0 σ above the image mean, after the image has been leveled by the model.

Semiautomated Segmentation of GA: Initial Image

A core of GA was defined on the initial image by taking a single user-selected threshold on a Gaussian filtered (35-μm radius) copy of the AF image. The filter was applied to remove inhomogeneities in the original and allow a smooth selection. The threshold was chosen to maximize capture of the lesion without going beyond the boundary. The core of GA was then masked, whereas the background of the remainder of the filtered image was modeled with the 12-zone mathematical model. The filtered image was then leveled by subtracting the background model as just described for the normal images. Remaining areas of decreased fluorescence in addition to the core were then defined globally by the lower of the two Otsu thresholds applied to the leveled image (Fig. 2). These additional areas were combined with the original core of GA to yield the complete segmentation of GA for this

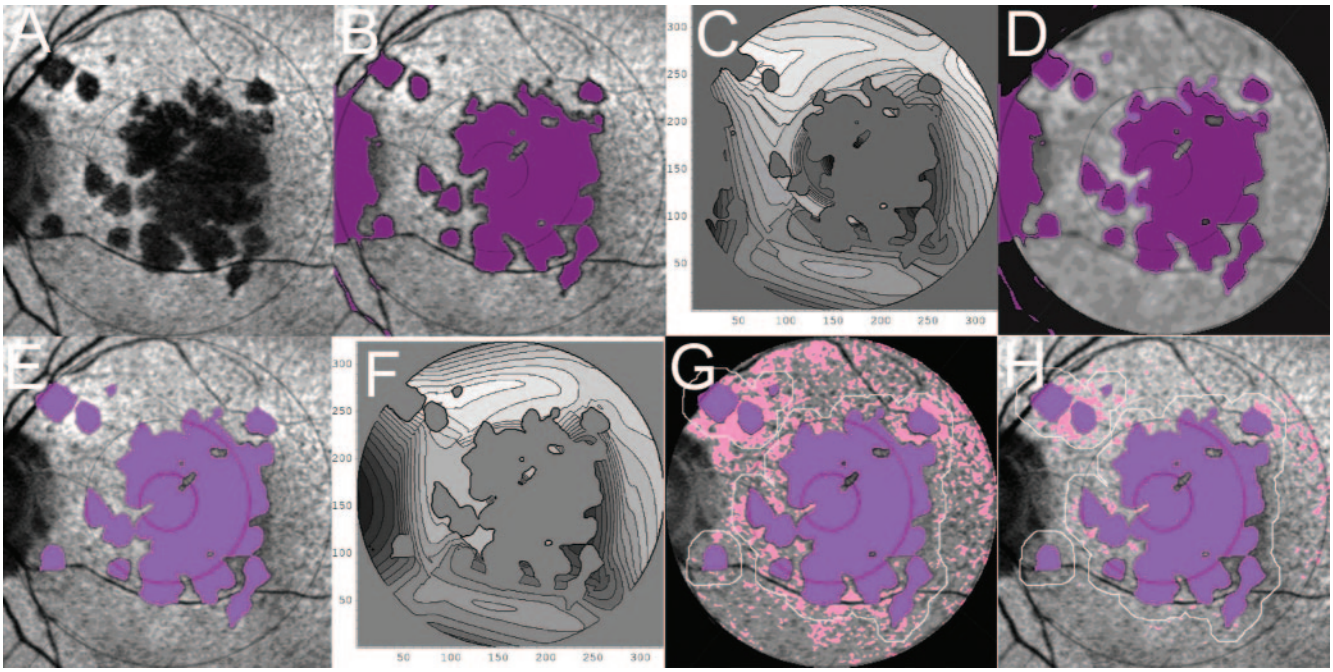

FIGURE 2. Semiautomated GA segmentation and automated increased FAF segmentation. (**A**) Initial AF image, patient 2 OS. (**B**) GA core (*dark purple*) defined by a user threshold applied to Gaussian-filtered original. The threshold is chosen so that as much of the lesion is captured without going beyond the boundary. In this case, the GA lesion is captured up to the boundary temporally, but there are still dark bands remaining nasally. (**C**) The mathematical model of the AF image in (**A**) after masking the GA core and filtering. (**D**) The filtered original was leveled by subtracting the mathematical model in (**C**). Additional bands of GA (*purple*) were then detected nasally and combined with the GA core, to complete the GA segmentation. (**E**) Original with complete GA (now all *purple*) masked. Extraneous vessel fragments and the optic nerve have been removed manually. (**F**) The mathematical model of the AF image in (**E**) after masking the GA. (**G**) The image in (**E**) was leveled by the mathematical model. Increased FAF could now be defined as any multiple of the leveled image SD above the leveled image mean. For illustration, increased FAF (*pink*) was defined as 1.0 SD above the leveled image mean and superimposed on the leveled image. The boundary zone is outlined in *white*. (**H**) Increased FAF was defined as 2.0 standard deviations above the mean (our usual definition) and superimposed on the original AF image, together with the GA segmentation. Less increased FAF is defined than in (**G**), but the pattern is roughly the same.

image. Occasional vessel fragments or peripapillary atrophy were removed manually.

Automated Increased FAF Segmentation: Initial Image

Areas of GA were first segmented as described previously and masked from the (nonfiltered) image to be leveled by the model. After recomputing the model and leveling the background of the remaining image, the mean and SD σ of the resultant leveled image were used to define the threshold for increased FAF. The threshold was set at 2.0 σ above the mean, to determine the total increased FAF in the image. A sensitivity analysis was also conducted to measure the impact of redefining increased FAF thresholds at 1.0 and 1.5 σ above the mean in four patients. The 250-μm border zone of the initial GA lesion was determined digitally by dilating the boundary in the image analysis software (Photoshop; Adobe Systems). We then studied only the increased FAF contained within the border zone and measured it as a percentage of this zone (Fig. 2).

For special situations in which GA consisted of a primary lesion associated with significant secondary lesions, analysis was conducted within expanded 250-μm border zones that circumscribed both primary and secondary lesions. We also considered a larger 500-μm border zone and performed all calculations for the increased FAF in this zone for six eyes of six subjects.

Sequential Segmentation of GA: Final Image

The initial and final AF images were registered on computer (Matlab 7.0; The Mathworks, Inc., Natick, MA). Because they were precisely superimposed, the area of GA from the initial image was used as a core of GA on the final image. After this core of GA was masked from the final image, the new areas of GA in the final image were found by leveling the remaining image and proceeding just as described previously for semiautomated GA segmentation.

Manual Tracing Method for GA

To verify our results with the semiautomated methodology, we also drew the boundaries of all GA lesions identified in the AF image with a 1-pixel pencil tool (Photoshop; Adobe Systems), outlining the lesions in a transparent digital layer. The lesions were verified to be GA by viewing the original slides according to standard criteria.[29–30] Reference was also made as needed to the fundus photographs to decide on the exact boundary. The lesion outlines were then filled, and their areas calculated.

Measurements

All areas of focally increased FAF (FIAF) and new GA (NGA) are expressed as decimal fractions of the border zone (i.e., numbers between 0 and 1). The positive predictive value (PPV) that pixels with increased FAF would become new GA (NGA) is given by

$$\mathrm{PPV} = \frac{\mathrm{p(FIAF} \cap \mathrm{NGA)}}{\mathrm{p(FIAF)}}.$$

This equation computes the probability that any pixel with increased FAF in the initial image becomes part of NGA in the final image. Thus, if every pixel with increased FAF becomes atrophic, the numerator and denominator become equal and PPV = 1. If half the increased FAF pixels become atrophic, then PPV = 0.5, and so on. The relative PPV (relPPV) is determined relative to the total quantity of NGA

$$\text{relPPV} = \frac{\text{PPV}}{\text{p(NGA)}} = \frac{\text{p(FIAF} \cap \text{NGA)}}{\text{p(FIAF)p(NGA)}}.$$

This equation more accurately reflects the strength of the predictive power. By random chance alone, the probability that any pixel falls into NGA is equal to the fractional area of NGA, or p(NGA). That is, the PPV of random guessing is exactly as good as the fractional area of NGA. Dividing by that quantity gives a relPPV, which is equal to one for random chance, and in general provides the predictive value *relative to chance*, expressed as a multiple.

The negative predictive value (NPV) of increased FAF—that is, that pixels *without* focally increased FAF (denoted ~FIAF) would *not* become atrophic (denoted ~NGA)—is given by

$$\text{NPV} = \frac{\text{p(}\sim\text{FIAF} \cap \sim\text{NGA)}}{\text{p(}\sim\text{FIAF)}}.$$

This equation calculates the probability that any pixel without increased FAF in the initial image will remain nonatrophic in the final image. Thus, if every pixel with normal AF remained nonatrophic, the numerator and denominator would become equal, with NPV = 1. If one third of the normal AF pixels become atrophic (i.e., only two thirds remain normal), then NPV = 0.67, and so on. The relative NPV (relNPV) is determined relative to the total quantity of nonatrophic pixels

$$\text{relNPV} = \frac{\text{NPV}}{\text{p(}\sim\text{NGA)}} = \frac{\text{p(}\sim\text{FIAF} \cap \sim\text{NGA)}}{\text{p(}\sim\text{FIAF)p(}\sim\text{NGA)}}.$$

By the same logic as for positive predictive power, this equation more accurately reflects the strength of the negative predictive power. By random chance alone, the probability that any pixel would remain nonatrophic is equal to the fractional area of nonatrophic pixels, or p(~NGA). That is, the NPV of random guessing is exactly as good as the fractional area of nonatrophic pixels. Dividing by that quantity gives a relNPV that is equal to 1 for random chance and in general provides the NPV *relative to chance*, expressed as a multiple.

An example of these calculations based on the segmentation processes is provided in Figure 3.

As another metric for comparison with the predictive value of increased FAF, we also considered the predictive value of proximity to the original GA lesion. In other words, in some patients, much of the NGA occurs close to the original lesion. We asked whether increased FAF was any better than proximity in predicting NGA. To find out, we considered the 500-μm border zone around the original GA and called those pixels that lay in the 250-μm border proximal and those that did not distal. This division into two subsets is analogous to the dichotomy of having, or not having, increased FAF. We then calculated the PPV, relPPV, NPV, and relNPV of being proximal with respect to the development of NGA in the 500-μm border zone. The eyes studied were the same six eyes from our six subjects that were studied in the 500-μm zone for the predictive value of increased FAF.

Results

When the manual tracings of the initial GA lesions were compared with those generated by the semiautomated method, the 95% limits of agreement[31] for all measured areas were −2.5% ± 3.9%, with the CI of the manual tracings slightly higher on average. The sensitivity and specificity of the semiautomated measurements with respect to the manual (ground truth) tracings ranged from 0.86 to 0.98 and from 0.95 to 0.98.

As a fraction of the 250-μm border zone, the mean NGA was 0.44 ± 0.20 and the mean increased FAF was 0.06 ± 0.06. The mean PPV of increased FAF for NGA formation was 0.40 ± 0.26. Compared with the relPPV of chance of 1.0, the mean relPPV of increased FAF was 1.15 ± 0.28. The mean NPV of increased FAF (i.e., that pixels without increased FAF would not become atrophic) was 0.57 ± 0.20, and the mean relNPV was 1.00 ± 0.02 (Table 1).

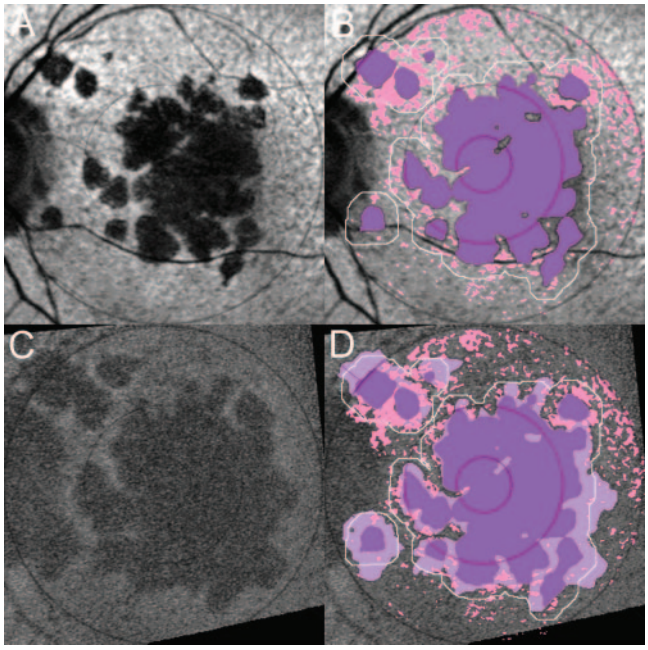

Figure 3. Predictive value of increased FAF for progression of GA. (**A**) Initial AF image, patient 2 OS. (**B**) Segmentation into GA (*purple*), with border zone outlined in *white*, and increased FAF (*pink*). Details of steps involved are in Figure 2. The increased FAF was defined as 1.5 standard deviations above the leveled image mean for this illustration. (**C**) Final AF image, 3 years later. The image is of only fair quality, but the GA is adequately defined. Note how the image has been stretched and rotated by the registration software to align with the initial image in (**A**). (**D**) The total GA is composed of NGA (*light purple*) and original GA (**B**, *purple*). The original increased FAF in (**B**) is superimposed, and 49% fell on NGA. The PPV of increased FAF for predicting NGA in the border zone was thus 0.49. NGA comprised 62% of the border zone. Hence, a random choice of pixels should predict NGA with 62% accuracy. Thus, the relPPV for increased FAF was 0.49/0.62 = 0.79, somewhat less than chance. The NPV of increased FAF (i.e., for predicting that NGA would not form in areas with normal AF), was 0.33 (relNPV 0.85, also somewhat less than chance). Varying the threshold for increased FAF had little impact (Table 3).

In the 500-μm border zone, the mean NGA was 0.25 ± 0.13, and the mean increased FAF was 0.05 ± 0.03. The mean PPV of increased FAF for NGA formation was 0.34 ± 0.14, and mean relPPV was 1.56 ± 0.70, and the mean NPV was 0.75 ± 0.13. The mean relNPV of increased FAF was 1.01 ± 0.01. The proximal pixels, defined as lying within 250 μm of the original GA lesion, comprised a mean fraction 0.58 ± 0.04 of this same 500-μm border zone. The mean PPV of being proximal for NGA formation was 0.38 ± 0.20, and the mean relPPV was 1.52 ± 0.26. The PPV and relPPV of increased FAF did not differ significantly from those of being proximal. The mean NPV of being proximal was 0.92 ± 0.06 and the mean relNPV was 1.26 ± 0.19. The NPV and relNPV of being proximal were significantly greater than the NPV and relNPV of increased FAF ($P = 0.01$ and $P = 0.02$, respectively, paired t-tests; Table 2).

Classification by FAF phenotype pattern[25] revealed a distribution of two diffuse branching, two diffuse fine granular, two focal, one diffuse fine granular with peripheral punctuate, and one banded (Table 1). For diffuse phenotypes, the mean relPPV of increased FAF was 1.01 ± 0.17 and the mean relNPV was 1.00 ± 0.03. For nondiffuse phenotypes studied (focal and

TABLE 1. Predictive Value of Increased FAF for Junctional GA Progression

Patient	Eye	FAF Phenotype	Duration between AF Images (years)	Increased FAF	New GA	PPV	Relative PPV	NPV	Relative NPV
1	OD	Diffuse branching	3	0.06	0.63	0.71	1.13	0.38	1.01
1	OS	Diffuse branching	3	0.04	0.34	0.32	0.94	0.66	1.00
2	OS	Diffuse fine granular with peripheral punctate	3	0.13	0.62	0.50	0.81	0.36	0.95
3	OS	Banded	2	0.15	0.11	0.12	1.06	0.89	1.00
4	OD	Diffuse fine granular	2	0.01	0.55	0.60	1.10	0.46	1.00
5	OS	Focal	3	0.02	0.17	0.20	1.15	0.83	1.00
5	OS	Focal	3	0.01	0.48	0.84	1.76	0.52	1.01
6	OD	Diffuse fine granular	3	0.10	0.58	0.72	1.24	0.44	1.04
Average			2.75	0.06	0.44	0.50	1.15	0.57	1.00
SD			0.46	0.06	0.20	0.26	0.28	0.20	0.02

Serial AF images of Eyes of Patients with AMD with GA were digitally analyzed. Areas of GA were identified on the initial image. Increased FAF was identified and measured as a percentage of the 250-μm border zone surrounding the initial GA lesion. Areas of GA were identified on the final image. PPV is the probability that pixels with increased FAF in the initial image became part of new GA in the final image. NPV is the probability that pixels without increased FAF did not become atrophic. Relative PV is the chance-adjusted predictive value. It is expressed as a ratio, compensating for the chance probability that any pixel that remained nonatrophic (or became atrophic) is equal to the fractional area of nonatrophic (or atrophic) pixels.

banded), the mean relPPV of increased FAF was 1.32 ± 0.38, and the mean relNPV was 1.00 ± 0.003.

DISCUSSION

The purpose of this study was to determine whether lipofuscin accumulation in AMD, as measured by increased FAF, precedes development of atrophy. This was achieved by digitally analyzing serial AF images from patients with AMD with GA.

The results of quantitative image analysis suggest that FAF is not a strong risk factor for development or extension of GA. Although areas of increased FAF may have modest positive and negative predictive values, the relative predictive values are generally no greater than chance.

When analyzed by phenotype subgroup, the predictive power of increased FAF remains similar. A previous study suggested that GA progression is more rapid in the diffuse FAF phenotype (Bindewald et al. *IOVS* 2004;45:ARVO E-Abstract 2960). Although our study did not focus on the rate of GA progression, our results demonstrate that increased FAF in the diffuse phenotype had negligible relative predictive values. Among the nondiffuse phenotypes examined (focal and banded), one patient (number 5) with the focal phenotype demonstrated bilateral GA progression in areas of increased FAF in a pattern similar to that reported by Holz et al.[24] This was also the only patient who had a relPPV (2.84) that was markedly greater than chance in the 500-μm border zone, and that was also significantly higher than the relPPV (1.26) of simple proximity to the original GA lesion. This finding suggests that there may be a distinct subset of GA patients in whom increased FAF is highly predictive of GA development, whereas in most patients it is not.

The total quantity of increased FAF in the border zone also does not appear to correlate with GA progression. Patient 1 OD had increased FAF of only 0.06 and developed NGA of 0.63, whereas patient 3 OS had increased FAF of 0.15 but developed NGA of only 0.11. This further suggests that although increased FAF and atrophy progression are both manifestations of disease, the former does not predict the latter.

A comment on the NPV of increased FAF is also in order. To what extent is the presence of normal background (not increased) FAF protective against the subsequent development

TABLE 2. Predictive Value of FAF Compared with that of Proximity to Original GA

		PPV		Relative PPV		NPV*		Relative NPV†	
Patient	Eye	FAF	Proximity	FAF	Proximity	FAF	Proximity	FAF	Proximity
1	OS	0.35	0.34	1.27	1.23	0.72	0.84	1.00	1.17
2	OS	0.33	0.56	0.82	1.41	0.60	0.86	0.99	1.43
3	OS	0.11	0.11	1.72	1.85	0.94	1.00	1.00	1.06
4	OD	0.35	0.52	1.12	1.65	0.69	0.94	1.00	1.37
5	OS	0.39	0.17	2.84	1.26	0.87	0.91	1.01	1.06
6	OD	0.53	0.58	1.57	1.72	0.68	0.97	1.03	1.47
Average		0.34	0.38	1.56	1.52	0.75	0.92	1.01	1.26
SD		0.14	0.20	0.70	0.26	0.13	0.06	0.01	0.19

Serial AF images from eyes of patients with AMD with GA were digitally analyzed. Areas of GA were identified on the initial image. Increased FAF was identified and measured as a percentage of the 500-μm border zone surrounding the initial GA lesion. Areas of new GA were identified on the final image in the 500-μm border zone. PPV (or NPV) for increased FAF is the probability that pixels with (or without) increased FAF became (or did not become) atrophic in the 500-μm zone. Relative PPV (or NPV) for increased FAF compensates for the chance probability that any pixel that became (or did not become) atrophic is equal to the fractional area of atrophic (or nonatrophic) pixels in the 500-μm zone. PPV (or NPV) for proximity is the probability that pixels within (or distal to) the 250-μm border zone became (or did not become) atrophic. Relative PPV (or NPV) for proximity is the PPV (or NPV) normalized by the fractional area of atrophic (or nonatrophic) pixels in the 500-μm zone, just as was done for the relative PPV (or NPV) of increased FAF.

* Statistically significant difference between NPV for proximity and FAF ($P = 0.01$).

† Statistically significant difference between relative NPV for proximity and FAF ($P = 0.02$).

TABLE 3. Sensitivity of Predictive Values to Standard Deviation Threshold Used to Define Increased FAF in Selected Patients

Patient	Eye	Duration between AF Images (years)	SD	Increased FAF	Relative PPV	Relative NPV
1	OS	2	2.0	0.04	0.72	0.99
			1.5	0.08	0.67	0.99
			1.0	0.15	0.77	0.93
2	OS	3	2.0	0.13	0.81	0.95
			1.5	0.29	0.79	0.86
			1.0	0.42	0.81	0.78
4	OD	2	2.0	0.01	1.10	1.00
			1.5	0.02	1.17	1.00
			1.0	0.05	1.05	1.00
5	OS	3	2.0	0.02	1.15	1.00
			1.5	0.05	0.97	1.00
			1.0	0.11	0.84	1.00

Pixels were defined to have increased FAF if their gray levels were greater than 2.0 standard deviations above the image mean. The standard deviation threshold used to define increased FAF was varied to measure the impact on predictive values.

of NGA? In our results this was measured by the relNPV, which approximated that of random chance (1.0) with a striking uniformity (Tables 1, 2, 3). One is forced to conclude that other disease processes not measured by increased FAF are driving the development of GA. In contrast, the metric of proximity to the original GA lesion was minimally to moderately superior to chance in all cases. This is consistent with the generally accepted notion that, whatever disease processes cause GA, they proceed centrifugally rather than evenly in the macula, with greater protection in areas furthest from the original GA lesion.

It is important to point out that this analysis, although providing an alternative viewpoint to other theories about increased FAF and GA in AMD, is not inconsistent with the large body of circumstantial evidence implicating lipofuscin as causative in retinal diseases. Increased FAF is defined relative to background fluorescence levels, whereas a generalized background elevation of fluorescence attributable to lipofuscin could be a better correlate.

Our study has several limitations. First, it was a retrospective study of eight eyes in six patients, which may not be representative of the population with GA. The existing literature is confined to a prospective case series of three patients drawn from a much larger group due to limitations of image quality. In each study, there could be some selection bias. Both studies rejected images of poor quality. We required good quality in the initial images so that increased FAF would be well characterized. We allowed fair quality in the final image if the GA could be well defined and there were sufficient details for image registration (Fig. 3C).

Second, images were derived from the HRA software, which registers and averages multiple individual AF scans. In each case, the number of scans averaged may differ due to scan quality and availability, resulting in differences in image dynamic range and signal-to-noise ratio. As just discussed, we maintained standards for image quality.

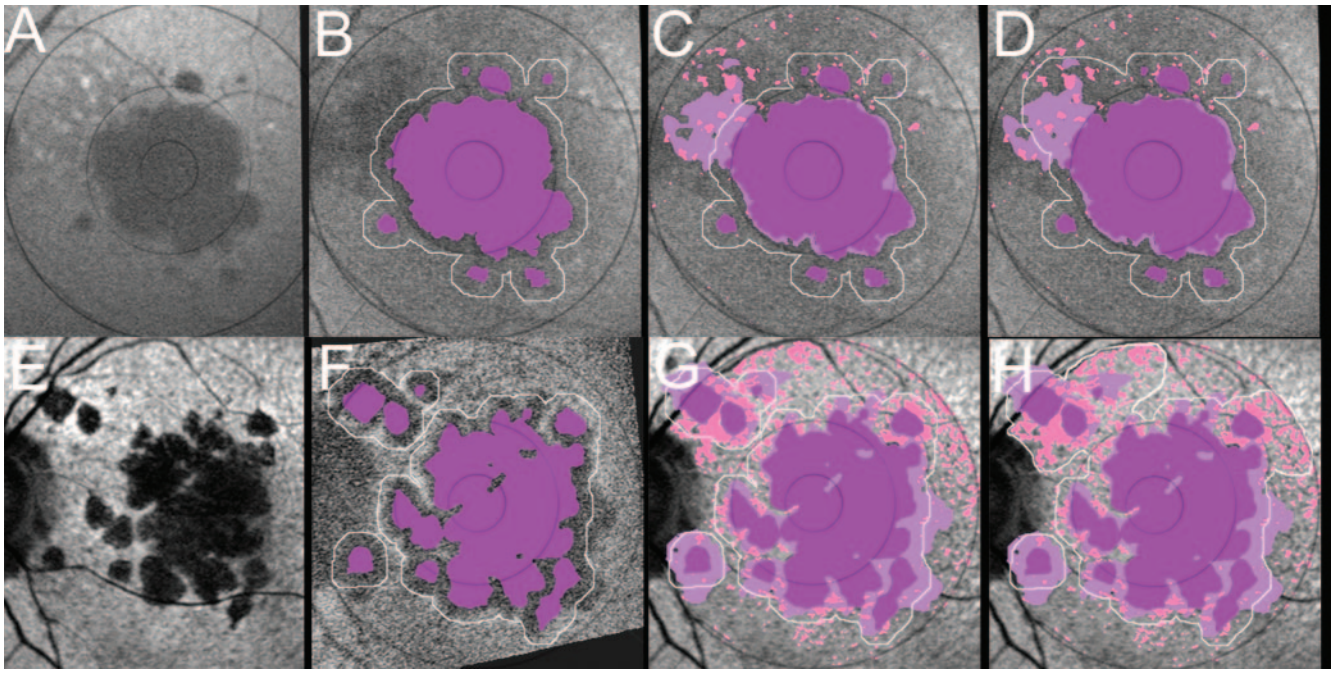

FIGURE 4. The effect of including additional increased FAF outside the GA border zone on the predictive value of increased FAF. *Top row*: patient 5 OS; *bottom row*: patient 2 OS. (**A**, **E**) The initial AF scans. (**B**, **F**) The 3-year follow-up scans with the initial GA superimposed in *purple*. The 250-μm border zone is outlined in *white*. (**C**) NGA in patient 5 OS (*light purple*) is identified on the follow-up scan, most prominently superonasal. The increased FAF on the initial scan (*pink*) is superimposed. The relPPV (PPV) of increased FAF in the border zone was 1.15 and the relNPV (NPV) was 1.00. (**D**) The border zone was enlarged to include increased FAF and NGA superonasally. The relPPV improved to 1.56, somewhat better than chance (1.00). The relNPV was unchanged (1.01). G. NGA in patient 2 OS (*light purple*) was identified in the border zone on the follow-up scan in all quadrants. The increased FAF on the initial scan, defined as 1.5 standard deviations above the leveled image mean to capture more of the increased FAF for this illustration (*pink*), is superimposed. Note large areas of NGA not associated with increased FAF. The relPPV of increased FAF in the border zone was 0.79, and the relNPV was 0.86. (**H**) The border zone was enlarged to include additional prominent increased FAF in the superior quadrants. However, there was no significant NGA in these areas. The relPPV and NPV declined further to 0.69 and 0.83, respectively. These results were not significantly different for increased FAF defined as 2.0 standard deviations above the mean.

Third, increased FAF was defined to be two standard deviations above the mean image intensity in the leveled image. We chose this level based on our study of normal images, in which this definition resulted in minimal increased FAF (<0.3% of pixels). Although it is possible that another definition could have changed the calculated predictive values, a sample set of calculations in four sets of serial images in which increased FAF was defined as 1.0 or 1.5 standard deviations above the mean gave virtually identical results (Table 3).

Fourth, results were somewhat dependent on the border zone surrounding the initial GA lesion chosen to represent the junctional zone. For example, in two patients with significant areas of increased FAF outside the original 250-μm border zone, a locally expanded border was used to measure the impact on predictive values (Figs. 4D, 4H). One patient demonstrated an insignificant change in relNPV and a modest increase in PPV. The second patient demonstrated a decrease in relNPV and PPV. More systematically, six eyes of six patients were analyzed in a uniformly expanded 500-μm border zone. The relPPV of increased FAF improved in each case, but in all but one case, the metric of proximity to the original GA lesion was a better predictor of NGA development (Table 2).

Our analysis expands on a pilot study conducted by Holz et al.,[24] which used largely qualitative methods to document atrophy progression in a small series of three GA patients. Our methodology builds on Holz's work by quantifying GA and lipofuscin accumulation at the pixel level, conferring precision and standardization. These benefits are particularly notable for the image-intense, technology-driven specialty of ophthalmology and should assist in elucidating the precise relationship between lipofuscin and retinal disease.

References

1. Feeney-Burns L, Berman ER, Rothman H. Lipofuscin of human retinal pigment epithelium. *Am J Ophthalmol.* 1980;90:783–791.
2. Katz ML, Gao CL, Rice LM. Formation of lipofuscin-like fluorophores by reaction of retinal with photoreceptor outer segments and liposomes. *Mech Ageing Dev.* 1996;92:159–174.
3. Kennedy CJ, Rakoczy PE, Constable IJ. Lipofuscin of the retinal pigment epithelium: a review. *Eye.* 1995;9:763–771.
4. Weiter JJ, Delori FC, Wing GL, Fitch KA. Retinal pigment epithelial lipofuscin and melanin and choroidal melanin in human eyes. *Invest Ophthalmol Vis Sci.* 1986;2:145–152.
5. Sparrow JR, Boulton M. RPE lipofuscin and its role in retinal pathobiology. *Exp Eye Res.* 2005;80:595–606.
6. Boulton M, McKechnie M, Breda J, Bayly M, Marshall J. The formation of autofluorescent granules in cultured human RPE. *Invest Ophthalmol Vis Sci.* 1989;30:82–89.
7. Young RW. Pathophysiology of age-related macular degeneration. *Surv Ophthalmol.* 1987;31:291–306.
8. Dorey KC, Wu G, Ebenstein D, Garsd A, Weiter JJ. Cell loss in aging retina: relationship to lipofuscin accumulation and macular degeneration. *Invest Ophthalmol Vis Sci.* 1989;30:1691–1699.
9. Holz FG, Schuett F, Kopitz J, et al. Inhibition of lysosomal degradative functions in RPE cells by a retinoid component of lipofuscin. *Invest Ophthalmol Vis Sci.* 1999;40:737–743.
10. Zhou J, Cai B, Jang YP, Pachydaki S, Schmidt AM, Sparrow JR. Mechanisms for the induction of HNE- MDA- and AGE-adducts, RAGE and VEGF in retinal pigment epithelial cells. *Exp Eye Res.* 2005;80:567–580.
11. Sparrow JR, Fishkin N, Zhou J, et al. A2E, a byproduct of the visual cycle. *Vision Res.* 2003;43:2983–2990.
12. Frangieh GT, Green R, Fine SL. A histopathological study of Best's macular dystrophy. *Arch Ophthalmol.* 1982;100:1115–1121.
13. Weiter JJ, Delori FC, Wing GL, Fitch KA. Retinal pigment epithelial lipofuscin and melanin and choroidal melanin in human eyes. *Invest Ophthalmol Vis Sci.* 1986;27:141–152.
14. O'Gorman S, Flaherty WA, Fishman GA, Berson EL. Histopathologic findings in Best's vitelliform macular dystrophy. *Arch Ophthalmol.* 1998;106:1261–1268.
15. Delori FC, Fleckner MR, Goger DG, et al. Autofluorescence distribution associated with drusen in age-related macular degeneration. *Invest Ophthalmol Vis Sci.* 2000;41:496–504.
16. Delori FC, Dorey CK, Staurenghi G, et al. In vivo fluorescence of the ocular fundus exhibits retinal pigment epithelium lipofuscin characteristics. *Invest Ophthalmol Vis Sci.* 1995;36:718–729.
17. Rückmann AV, Fitzke FW, Bird AC. Distribution of fundus autofluorescence with a scanning laser ophthalmoscope. *Br J Ophthalmol.* 1995;79:407–412.
18. Rückmann AV, Fitzke FW, Bird AC. Fundus autofluorescence in age-related macular disease imaged with a laser scanning ophthalmoscope. *Invest Ophthalmol Vis Sci.* 1997;38:478–486.
19. Klaver CC, Wolfs RC, Vingerling JR, Hofman A, de Jong PT. Age-specific prevalence and causes of blindness and visual impairment in an older population: the Rotterdam Study. *Arch Ophthalmol.* 1998;116:653–658.
20. Maguire P, Vine AK. Geographic atrophy of the retinal pigment epithelium. *Am J Ophthalmol.* 1986;102:621–625.
21. Sarks JP, Sarks SH. Killingworth MC. Evolution of geographic atrophy of the retinal pigment epithelium. *Eye.* 1988;2:552–577.
22. Klein R, Klein BE, Jensen SC, et al. The five-year incidence and progression of age-related maculopathy: the Beaver Dam Eye Study. *Ophthalmology.* 1997;104:7–21.
23. Sunness JS. The natural history of geographic atrophy, the advanced atrophic form of age-related macular degeneration. *Mol Vis.* 1999;5:25–29.
24. Holz FG, Bellmann C, Staudt S, et al. Fundus autofluorescence and development of geographic atrophy in age-related macular degeneration. *Invest Ophthalmol Vis Sci.* 2001;42:1051–1056.
25. Bindewald A, Bird AC, Dandekar SS, et al. Classification of fundus autofluorescence patterns in early age-related macular disease. *Invest Ophthalmol Vis Sci.* 2005;46:3309–3314.
26. Smith RT, Chan JK, Nagasaki T, et al. Automated detection of macular drusen using geometric background leveling and threshold selection. *Arch Ophthalmol.* 2005;123:200–206.
27. Smith RT, Koniarek JP, Chan J, Nagasaki T, Sparrow JR, Langton K. Autofluorescence characteristics of normal foveas and reconstruction of foveal autofluorescence from limited data subsets. *Invest Ophthalmol Vis Sci.* 2005;46:2940–2946.
28. Otsu N. A threshold selection method from gray-level histograms. *IEEE Trans Syst Man Cybern.* 1979;9:62–66.
29. Bird AC, Bressler NM, Bressler SB, et al. An international classification and grading system for age-related maculopathy and age-related macular degeneration. The International ARM Epidemiological Study Group. *Surv Ophthalmol.* 1995;39:367–374.
30. Klein R, Davis MD, Magli YL, Segal P, Klein BE, Hubbard L. The Wisconsin age-related maculopathy grading system. *Ophthalmology.* 1991;98:1128–1134.
31. Bland JM, Altman DG. Statistical methods for assessing agreement between two methods of clinical measurement. *Lancet.* 1986;1:307–310.